# Meteorological Application of an Instrumented Unmanned Aircraft System: Structure Function Parameters and Sodar Comparison


## Student Team

**David Goines**

*University of Oklahoma*

*School of Meteorology*

**Aaron Scott**

*University of Oklahoma*

*School of Meteorology*

## Mentors

**Dr. Phillip Chilson**

*Professor University of Oklahoma*

*School of Meteorology*

*Advanced Radar Research Center*

**Tim Bonin**

*University of Oklahoma*

*School of Meteorology*

*Advanced Radar Research Center*



Journal: Boundary-Layer Meteorology

6 May 2013

**Abstract**

The ability to obtain meteorological measurements in the planetary boundary layer for quantification of clear-air turbulence is investigated using the Small Multifunction Research and Teaching Sonde (SMARTSonde). With an instrumented unmanned aircraft, a series of flights were conducted in the spring of 2013 to obtain meteorological variables at Kessler Atmospheric and Ecological Field Station (KAEFS) near Purcell, Oklahoma. Flying in step-wise helical ascent patterns allows for the calculation of the temperature structure function parameter, $C_T^2$. A series of varying methods of calculation are used to examine which provides a more robust result. Given that the flights were conducted near remote sensing instruments, data collected are compared to sodar by a comparison of return power. This results in the possibility for verification of remote sensors by in-situ measurements from an unmanned aircraft system (UAS).

## Introduction

### *UAS Meteorological Capabilities*

Many years before the use of radio-controlled aircraft, the collection of in-situ measurements was primarily done with balloons, towers, and tethersondes (Bonin 2011). However, the collection of data with a reusable and moving platform that is able to acquire numerous data sets is very desirable to the meteorological community due to the research possibilities. The process of using radio controlled aircraft to gather atmospheric data has been ongoing since the 1970s (Konrad et al. 1970). However, it did not gain popularity within the meteorological community due to the bulky instrumentation that was available. In recent years, sensors have become much smaller and can now easily be deployed in a UAS (Unmanned Aircraft System). This has allowed for further application of these systems in the atmospheric sciences. With the use of UAS in meteorology, measurements of temperature, humidity, pressure, and other variables can be obtained at different levels. Unlike manned aircraft, unmanned aircraft are able to fly more safely and efficiently at low altitudes. They also allow a safe method of obtaining low level measurements within tight flight patterns, as such were needed for this project.

*Motivation*

The PBL (Planetary Boundary Layer) is the layer of atmosphere from the surface of the Earth to the stably stratified region leading to the free atmosphere (Wyngaard 1986). The depth of the PBL typically ranges from a few hundred to a few thousand meters as the day progresses (Lenschow 1986). The heating of the Earth's surface during the daylight hours in the PBL leads to vigorous turbulence that mixes the atmosphere while the depth of the PBL grows. After loss of daytime heating, turbulent mixing decreases in intensity and a new stably stratified layer forms near the surface and very little mixing takes place (Wyngaard 1986). These transitions of the PBL cause it to be very dynamic and difficult to forecast. Understanding the PBL can significantly impact humans. Anthropogenic air pollutants are occasionally trapped within the PBL because of a lack of mixing. An estimated two million deaths annually are associated with poor air quality (World Health Organization 2009). Having accurate sampling of this layer can help forecast the small scale, local flow that controls the movement of these pollutants.

Understanding the PBL can also help to improve atmospheric forecasts. The PBL is a critical component in the Earth-Atmospheric system. The rest of the atmosphere is affected by PBL processes, which are directly due to interactions with Earth's surface. Improvements in boundary-layer parameterization schemes are needed for numerical weather prediction models to help increase reliability and improve data assimilation for initial conditions. Moreover, with the availability of better initial conditions, more accurate weather forecasts can be formulated during high-risk weather events. For example, convective initiation relies heavily on PBL processes as relatively small changes can dictate when initiation of convection will occur or not occur (Crook 1996). Improving the forecast of high-risk severe weather events can greatly impact human life as hundreds are killed each year in the United States by severe weather.

Collecting measurements, from within the PBL, can help meteorologists understand the on-going turbulent mixing. Remote sensors, such as sodar and radar, provide a way of remotely probing the boundary layer

as a means of investigating its dynamic and thermodynamic properties and how they evolve over time. Using remote sensors, turbulent eddies can be detected through the effects of Bragg scattering (Gossard et al. 1982), which is related to the structure function parameter. Konrad et al. (1970) suggests that field experiments, relating to Bragg scattering processes caused by turbulent mixing, would require fast response instruments and a fine-scale measurement of the atmosphere. This paper utilizes Konrad's suggestion and explores the feasibility of using a UA to detect variations in meteorological variables in order to quantify clear air turbulent eddies and relate them to the reflectivity from remote sensors.

*Research Configuration*

At the University of Oklahoma, in conjunction with the Advanced Radar Research Center (ARRC), a project was begun in 2009 that focused on the use of a UAS to conduct studies within the PBL and assist with radar research (Chilson et al. 2009). The project, called the Small Multifunction Autonomous Research and Teaching Sonde (SMARTSonde), was closely designed after a Norwegian research group's concept, called SUMO (Small Unmanned Meteorological Observer) (Reuder et al. 2009). The SMARTSonde project utilizes an off-the-shelf R/C (Remote Control) aircraft, the Multiplex Funjet. The Funjet is made out of foam and utilizes a pusher prop design, which keeps the backwash of the propeller from affecting the sensors. The Funjet is quite agile and is usually hand launched and lands on the underside of the fuselage. Even with these capabilities, the airframe is quite stable during low speed flight allowing for reliable data collection. All of this allows the Funjet to be used in areas where a runway or large, open takeoff and landing space are not available.

The Funjet has the capability of fully autonomous flight. The entire autopilot system consists of a ground control station (GCS), the aircraft mentioned above, and a radio controller (Figure 1). The GCS communicates with the aircraft and displays the status of the Global Position System (GPS) location, battery level, and attitude. Autonomous flight is achieved using the Paparazzi autopilot system. Paparazzi is free open-source software developed by the French Civil Aviation University (Ecole Nationale De L'Aviation Civile) (Chilson et al. 2009). In autopilot mode, the Paparazzi system completely controls the aircraft's thrust, pitch, and roll. The system utilizes preprogrammed flight plans that can be created before a mission. The GCS is used to execute various stages of a flight plan and allows for limited changes while the aircraft is in flight. However, the hand held radio controller also allows the Funjet to be manually controlled at any moment during flight.

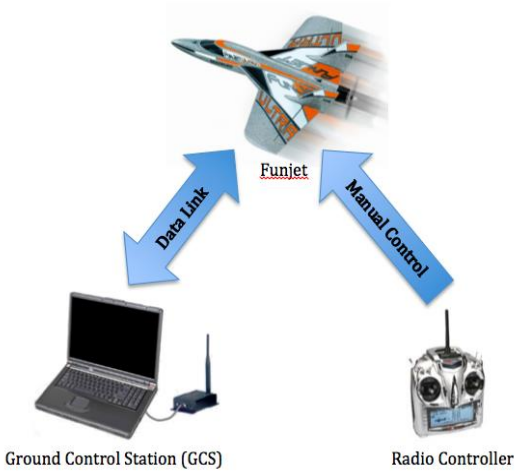


**Figure 1:** SMARTSonde project configuration.

The Funjet is outfitted with meteorological sensors and capable of measuring temperature, pressure, humidity, wind speed, and wind direction. The temperature and humidity sensor is located in an aspirated plastic tube that is located under the right wing of the aircraft up against the fuselage. The sensor is the Sensiron SHT75, where a capacitive sensor is used for humidity and a band-gap sensor is used for temperature measurement. The response time is eight seconds with accuracy within 0.3 K for temperature and 1.8% for relative humidity. For pressure measurements, the SCP1000 is located inside the unsealed fuselage and is capable of resolving pressure changes greater than 0.015 hPa.

Data were gathered at KAEFS (Kessler Atmospheric and Ecological Field Station) near Purcell, Oklahoma in McClain County. KAEFS is owned and maintained by the University of Oklahoma and is home to several research studies conducted by federal, state, and university researchers. The field station is an ideal location for this project because of the vast, open space with a sparse population in the surrounding area, and has

an on-site lidar and sodar that is maintained by the OU School of Meteorology. For further information about the facility, visit http://kaefs.ou.edu/.

In order to carry out legal operation of UA within the National Airspace, the University of Oklahoma obtained the state of Oklahoma's first Certificate of Authorization (CoA) from the Federal Aviation Administration (FAA) for civilian operation. This CoA, 2012-CSA-57, allows for unmanned aircraft flights at KAEFS within a one nautical mile radius and up to an altitude of 3000 feet given that a licensed pilot-in-command (PIC) is present along with four spotters. These spotters are required to have ground training and Class II medical certificates. Due to this requirement, both authors of this project took part in ground training and received Class II medical certificates. The team was also required to have the PIC in constant contact with the four spotters which were evenly spread across the flight area (Figure 2). The regulations of the CoA also restricts the aircraft to 500 feet below cloud level and the aircraft must land if another aircraft enters the CoA airspace.

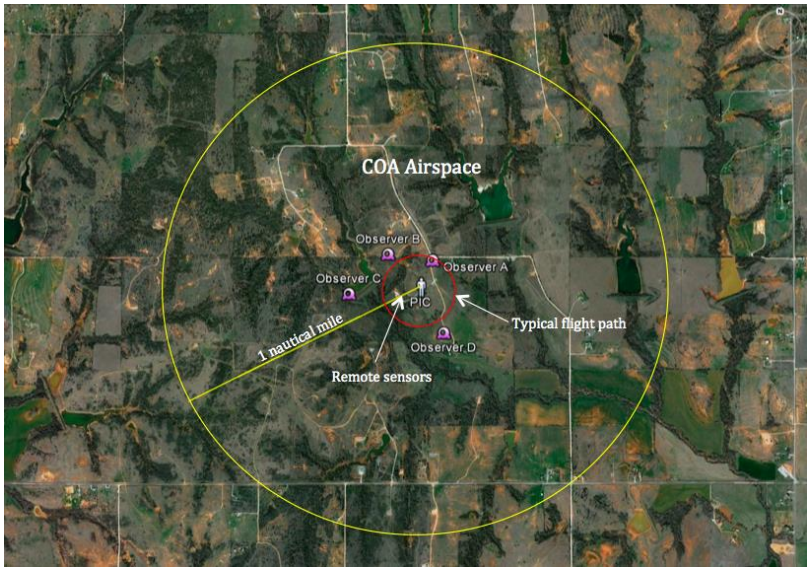


**Figure 2:** Aerial view of COA at KAEFS. Shows placement of PIC, four observes,typical flight path (red), COA airspace radius (yellow), and location of remote sensors. The height of the airspace is 3000 feet.

Flights at KAEFS consisted of a circular, step-wise, helical ascent that maintained level flight for roughly three minutes at incremental heights (Figure 3). A circular flight was necessary to keep the Funjet near the on-site remote sensors to ensure they were sampling approximately the same space. The step-wise circular flight, stopping at various incremental heights, allowed for multiple complete circular paths before ascending to the next

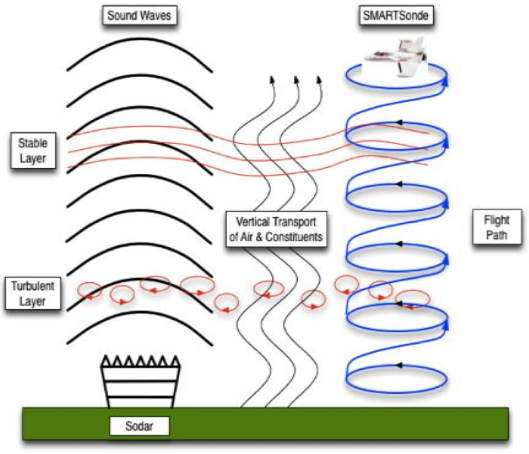


**Figure 3:** Schematic of typical data collection mission.

level. This allowed for estimation of turbulence parameters as discussed below. Once the peak altitude was reached, a controlled, slow descent down to the surface was used to capture a complete atmospheric profile of thermodynamic and dynamic parameters.

## Background

### *A Brief History of UA in Meteorology*

As mentioned previously, the idea of using radio controlled aircraft has been considered for some forty years. However, in has only been within the last two decades that a push for autonomous aircraft for meteorological purposes has emerged. Starting in the 1990s, the first autonomous UAS to take meteorological measurements, presented in the formal literature, was used in the Atmospheric Remote Sensing and Assessment Program (Stephens et al. 2000). In Australia, the development of the Aerosonde was first discussed by Holland et al. (1992). The platform was capable of measuring temperature, humidity, pressure, trace gas concentrations, and wind among others. It was used in several meteorological field projects including the Maritime Continent Thunderstorm Experiment (Schafer et al. 2001). The Aerosonde platform was also used as the first UA to penetrate a typhoon eyewall (Lin 2006).

Researchers in Germany have developed the Meteorological Mini-UAV ($M^2$ AV) to collect turbulence and wind vector measurements within the planetary boundary layer (Spiess et al. 2007). The data collected by Spiess et al. (2007) have also been compared with remote sensors including both a sodar and lidar. The comparisons yielded accurate results when compared to the remote sensors with the sodar comparing virtual temperature to the UAS and the lidar comparing absolute humidity to the unmanned aircraft.

In China, the Robotic Plane Meteorological Sounding System (RPMSS), was developed to acquire atmospheric soundings and thermodynamic profiles in remote areas of China (Shuqing et al. 2004). Using UAS in remote locations, such as China, demonstrates that their use in the atmospheric sciences could have significant

impact on the future of weather prediction since it allows important meteorological variables to be collected in areas that would otherwise remain void of measurement probing.

In the United States, efforts towards gathering meteorological in-situ measurements have been increasing since the late 2000s. The Collaborative Colorado-Nebraska UAS Experiment (CoCoNUE) was the first program in the United States entirely dedicated to collecting data within the planetary boundary layer over land (Houston et al. 2012). CoCoNUE carried out missions to collect data for mesoscale phenomena mainly focusing efforts on airmass boundaries.

Unmanned aircraft have proven to be a viable option to collect basic meteorological variables. As mentioned in the introduction, obtaining the structure function parameter for temperature with an unmanned aircraft could be useful for understanding turbulence. This was done in Germany with the $M^2$ AV (van den Kroonenberg et al. 2011). In their paper, a UAS was flown in straight paths in close proximity to a 99 meter tall meteorological tower. The temperature structure function parameter was obtained from both the $M^2$ AV and the sonic anemometer placed on the tower. The structure function was calculated using a moving window within which the temperature difference was calculated.

*Theory*

The vertical structure of the atmosphere typically exhibits significant changes in temperature, pressure, and humidity with height. While the horizontal characteristics in these variables are more homogenous, the presence of turbulent eddies may create small variations in these variables. The use of remote sensors in clear air sometimes results in backscatter from these horizontal gradients. According to Neff and Coulter (1986), if turbulence is locally isotropic and homogenous, the backscatter of acoustic waves, due to the horizontal gradient in temperature, can correspond to Bragg scattering. Bragg scattering also occurs to electromagnetic waves due to small inhomogeneities in the refractive index (Gossard et al. 1982). Atmospheric scientists have made use of both the scattering of acoustic and electromagnetic waves to obtain the structure of the PBL (Wyngaard et al. 1980).

However, this paper will only explore the Bragg scattering of acoustic waves. Attempting to quantify turbulence, using the aforementioned theories, begins with the structure function. According to Wyngaard (2010), the structure function of temperature is the average squared temperature, *T*, difference for separations of similar distance:

$$D_T^2 = < (\Delta T)^2 > \quad (1)$$

The <…> denotes ensemble averaging. If the turbulence being measured meets the four criteria of isotropic, homogeneous, volume filling, and within the inertial sub range, the structure function can be normalized using an inverse 2/3-law expression in separation distance (Kolmogorov 1941). The result yields the structure function parameter:

$$C_T^2 = \frac{D_T^2}{R^{2/3}} = \frac{<(\Delta T)^2>}{R^{2/3}} \quad (2)$$

where $\Delta T$ is the temperature difference, R is the separation distance between two points and <…> denotes ensemble averaging.

**Method**

The first step in analyzing the data is to find which data points coincide with constant flight levels. This is done manually by plotting the height above ground level from the GPS output for an entire flight. Data points associated with a constant height were then indexed to that height. Once these indices were found, the raw data at each height were analyzed to find erroneous values to ignore. For example, the collected meteorological variables were plotted with time to view the raw output from the sensors. By doing so, height fluctuations in the GPS location of the Funjet were noticed of approximately ±7 meters on average. As most afternoon flights occurred within a dry adiabatic atmosphere, potential temperature was hypothesized to correct for the height fluctuations. Potential temperature can be calculated using the following equation:

$$\theta = T\left(\frac{p_0}{p}\right)^{\frac{R_d}{C_p}} \quad (3)$$

where $T$ is temperature, $p$ is pressure, $R_d$ is the specific gas constant for air, and $C_p$ is the specific heat of dry air. This requires the pressure data from the Funjet to be utilized. A review of the raw pressure data led to the discovery of erroneous pressure spikes. This finding contributed to a decision to not use potential temperature in our analysis.

To calculate of the structure function for temperature, $D_T^2$, numerous squared temperature differences from points with equal separation distances of length R are averaged. For numerous and sporadic data points, such as the data obtained in this project, data points are likely never the same distance apart. Therefore, a binning process was utilized. The bin size used in this project was 20 m. For example, separation distances greater than 10 m and less than 30 m would be in the 20 m bin and separation distances greater than 30 m and less than 50 m would be in the 40 m bin, and so on. Average squared temperature differences will then be indexed to a respective bin. This process allows for a multitude of squared temperature differences to be averaged for a single separation distance. As mentioned in the background section of this paper, the structure function parameter can then be calculated using Equation 2. Figure 4 helps illustrate how structure function parameter for temperature was calculated in this project. Equation 4 and Equation 5 are examples of the calculation of the structure function parameters for temperature in the case of Figure 4. $R_n$ is separation distances and $T_n$ is temperature.

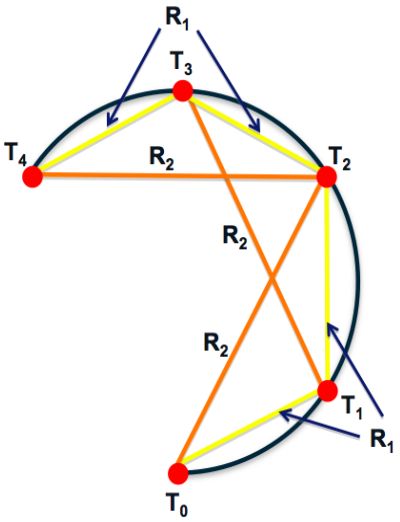


**Figure 4:** Example of a structure function parameter calculation.

$$C_T^2(R_1) = \frac{<(\Delta T)^2>}{R_1^{2/3}} = \frac{\left[\frac{(T_1-T_0)+(T_2-T_1)+(T_3-T_2)+(T_4-T_3)}{4}\right]^2}{R_1^{2/3}} \quad (4)$$

$$C_T^2(R_2) = \frac{<(\Delta T)^2>}{R_2^{2/3}} = \frac{\left[\frac{(T_2-T_0)+(T_3-T_1)+(T_4-T_2)}{3}\right]^2}{R_2^{2/3}} \quad (5)$$

This project examined two methods of calculating $C_T^2$. The first method uses all possible separation distances and temperature differences within the entire flight at a constant height. This even includes the difference between the first data point and the final data point, at a given height, roughly three minutes apart. This allows for a comparison between all data points around the sampled volume. However, this also may degrade the calculations of $C_T^2$ significantly because of the amount of time between data points. A long length of time between data allows for the advection of turbulence across the sampled volume. The Funjet is designed to fly a circular flight pattern over a stationary point, relative to the ground. Therefore, the advection of the turbulence needs to be accounted for in the calculation of $C_T^2$. This project utilized Taylor's hypothesis of frozen turbulence to compensate for the advection of turbulence (Taylor 1938). In Figure 5, R is the ground-relative separation distance between two data points with a time, Δt, apart. The variables x and y are the components of the GPS indicated separation distance. The mean wind speed has an x-component, u, and a y-component, v. Therefore, the effective location of temperature, $T_E(t+\Delta t)$, will be a distance of uΔt meters to the south and vΔt meters to the west of the GPS indicated temperature, T(t+Δt). The effective separation distance, $R_E$, can then be calculated by the following equation:

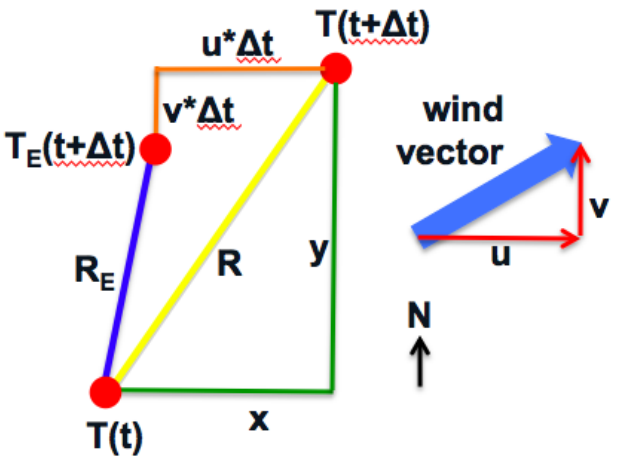


**Figure 5:** Schematic showing the implementation of Taylor's hypothesis of frozen turbulence

$$R_E = \sqrt{(x - u\Delta t)^2 + (y - v\Delta t)^2} \tag{6}$$

The second method used to calculate $C_T^2$ uses a technique described as the "moving window method". This method does not use all possible separation distances and temperature differences but only looks at the comparison between data points that are separated by a limited time period. This time limit was set as the time it takes the Funjet to complete one half of a circle. By doing so, you reduce the error of assuming data is

instantaneous. However, Taylor's hypothesis of frozen turbulence was still utilized for this method because of the length of time it takes to reach half way around the circle still allows for the advection of turbulence.

As mentioned in the Background, $C_T^2$ can be related to the Bragg scattering of acoustic waves. Therefore, $C_T^2$ was then used to calculate a proportional height corrected simulated reflectivity using the following equation:

$$\eta \propto \beta = \frac{{C_T^2}/{T^2}}{z^2} \tag{7}$$

where η is reflectivity, β is simulated reflectivity, $C_T^2$ is the structure function parameter for temperature, $T$ is the average temperature at a given height, and $z$ is height (Coulter and Wesely 1980). Many assumptions go into the use of this equation. Frist of all, $C_T^2$ is related to the Bragg scattering of acoustic waves, therefore, any other scattering medium in the sample space will create an error. Biological targets and other ground clutter may result in scattering other than Bragg scatter. Lastly, the computation of $C_T^2$ may not be adequate for the conditions present during data collection. If any of the four criteria needed, for structure function parameter theory, are not met in the sample space, $C_T^2$ will not be an accurate representation of the turbulence. Consequently, if the simulated reflectivity from the Funjet is proportional to the sodar reflectivity with height, all assumptions are correct. Therefore, proportionality between the sodar reflectivity and the Funjet simulated reflectivity allows for turbulent eddies to be accurately quantified with in-situ measurements.

## Results

### *Flight Overview*

Data for this project were collected during four separate days in the spring of 2013. Flights occurred on 14 March from 15:00 CDT to 17:00 CDT, 28 March from 07:00 CDT to 08:30 CDT, 11 April from 17:00 CDT to 18:30 CDT, and 24 April from 17:00 CDT to 19:00 CDT. However, the latter three days are being used for this paper due to GPS issues with the first round of flights on 14 March. On the morning of 28 March, three flights

were conducted at KAEFS starting just after sunrise. The data collected are unique as there was a noteworthy low-level jet (LLJ) approximately 400 m above ground level. The Funjet performed quit well within the LLJ although it did slow down to a 4 m $s^{-1}$ ground-level speed while travelling into the wind. A typical ground-relative speed was approximately 15 m $s^{-1}$. On 11 April and 24 April, several flights took place in the mid to late afternoon. Each of these three days concluded with three successful flights. However, there were a couple of instances in which a manned aircraft entered the CoA airspace, which caused termination of the flight, per CoA regulations. This resulted in data not being collected at all desired height levels.

Each flight consisted of a step-wise helical ascent followed by a controlled helical descent (Figure 6). The aircraft was flown manually during takeoff and was switched over to fully autonomous mode after a review of the system verified that the aircraft was safely operating. Level flights were maintained for roughly three minutes at each height increment. The Funjet preformed remarkably well during data collection compared to previous flights within the SMARTSonde project. It should be noted that flight trajectories, such as those depicted in Figure 6, represent the cumulative effort on the part of the current and previous members of the SMARTSonde team.

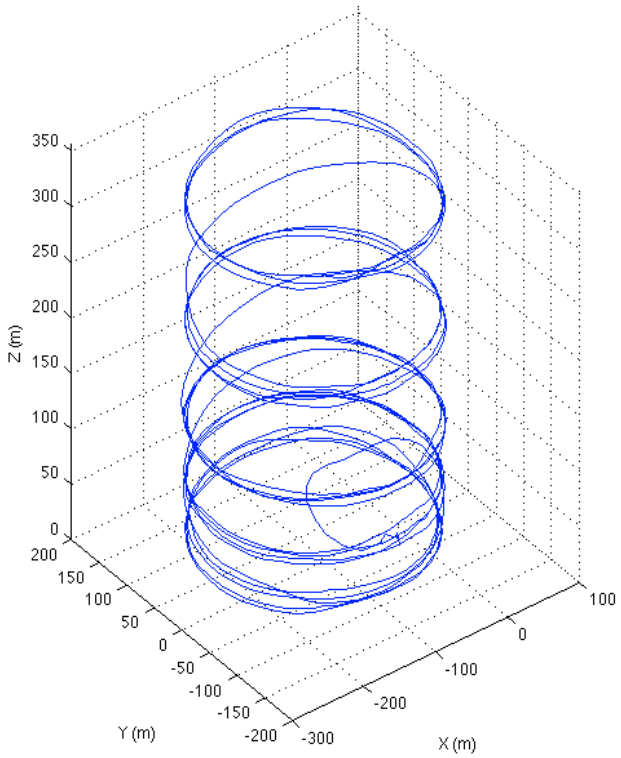


**Figure 6:** Step-wise helical ascent flight trajectory from the third flight on 11 April 2013.

*Atmospheric Profile*

Using the data collected, vertical profiles of the lower atmosphere were created to help visualize the condition of the PBL during our flights (Figure 7). The temperature profile from the morning of 28 March provides evidence of a nocturnal inversion. That morning, a LLJ was present and can be seen in the rightmost plot in Figure 7 where there appears to be a maximum wind speed of ~17 m $s^{-1}$ around 400 meters. The LLJ appears to be in close proximity to the top of the inversion where the temperature appears to become near isothermal again.

The temperature profiles on 11 April and 24 April 2013 suggest lapse rates were very near dry adiabatic. The wind speeds on both of these days were fairly uniform with height in the layer sampled by the Funjet with both days having maximum wind speeds of about 5 m $s^{-1}$. Relative humidity appeared to be fairly constant with height and then slightly decrease above 300m on 28 March. Relative humidity was fairly constant with height on both 11 April and 24 April, although, there was a slight increase with height on 11 April.

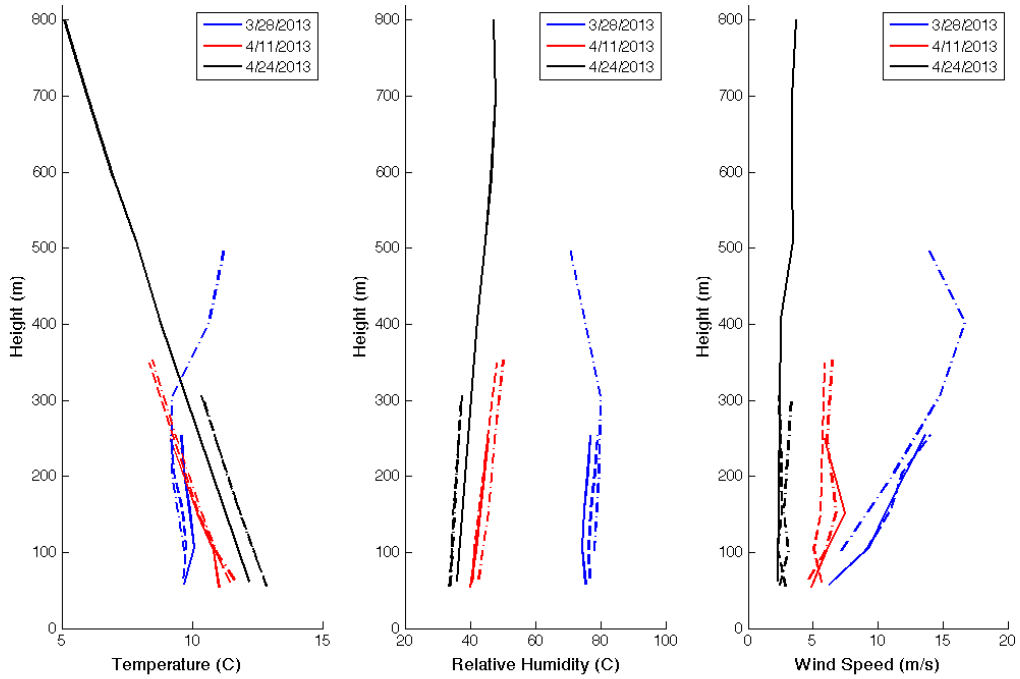


**Figure 7:** Temperature, relative humidity, and wind speed retrieved from the SMARTSonde from 3/28/2013 (Blue), 4/11/2013 (Red), 4/24/2013 (Black). Three flights were conducted each day. Flight 1 (solid), Flight 2 (dashed) Flight 3 (dash/dot).

Data collected as the UA completed circular paths at a given height are shown as a time-series in Figure 8. While we expect, on average, temperature to fluctuate with height, small temperature differences occurred over various horizontal distances. Although the Funjet did not maintain a perfect height while flying at the level it was instructed, it varied less than +/- 10 meters, on average. However, given the near dry adiabatic profile of the two afternoon cases, a small fluctuation in height, on the order of a few meters, would not cause a temperature difference greater than +/- 0.1 degrees Celsius. Given the time-series shown in Figure 8, the temperature fluctuations do not seem to coincide with the height fluctuations given a dry adiabatic lapse rate. Therefore, these temperature variations could be the product of turbulence.

In the lowermost graph of Figure 8, temperature was also plotted with respect to heading (direction). This was done on account of the concern that the low sun angles during flight could possibly affect the temperature data. During initial testing of the SMARTSonde, circular flights were counter-clockwise which puts the aircraft in a constant left turn. Since the temperature and relative humidity sensor are located under the wing on the right side of the aircraft, counter-clockwise circular flights put the sensor encasement tube partially in direct sunlight during afternoon hours when the UA was heading south. Therefore, the temperature data was experiencing oscillations that tended to be related to heading. To account for this, flights for this project were clockwise which puts the aircraft in a constant right turn. Therefore, the sensor encasement tube faced the ground and was shielded from the sun by the wing and fuselage. The lowermost graph in Figure 8 does not exhibit an oscillating pattern in temperature in relation to the heading, so it has been determined that solar radiation did not affect the temperature data.

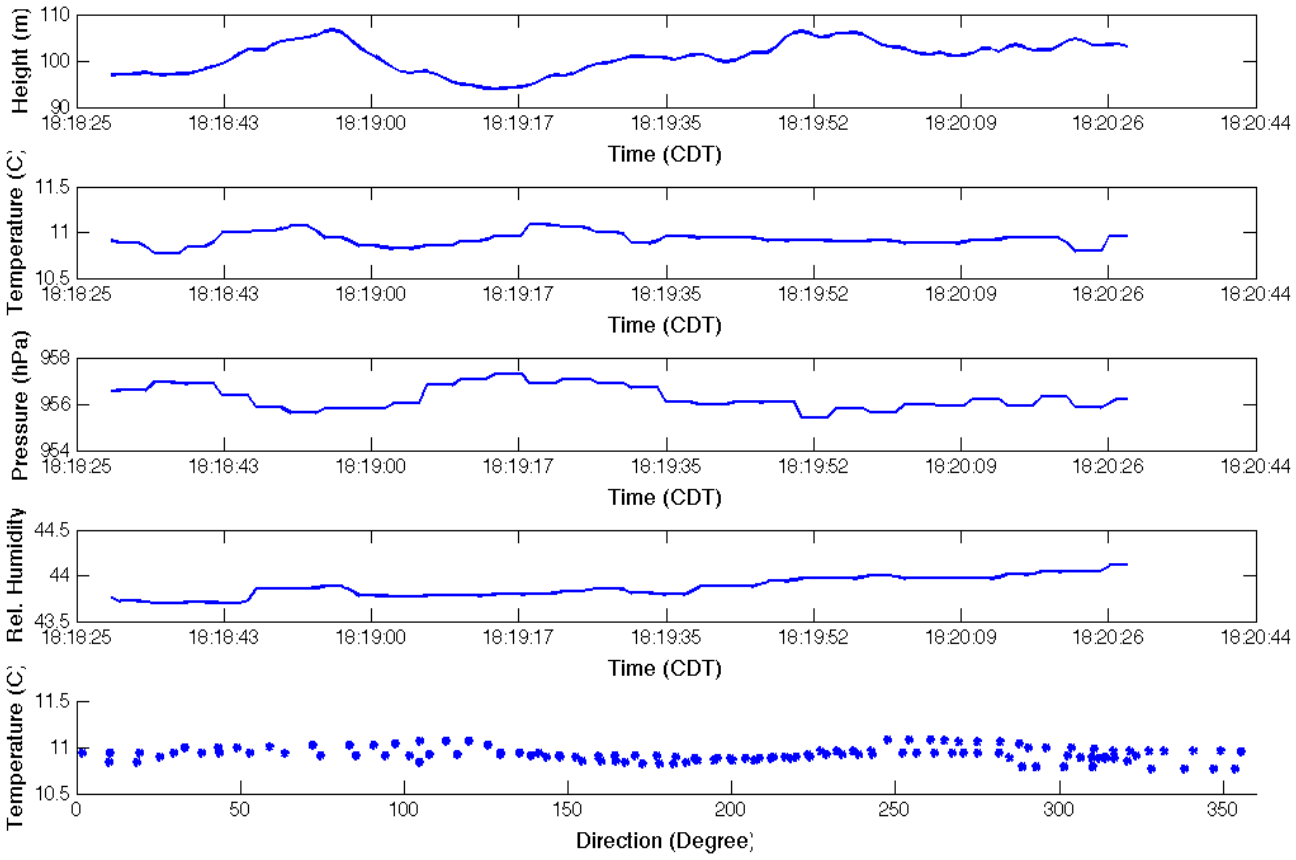


**Figure 8:** A time series of height, temperature, pressure, and relative humidity. The fifth figure also shows temperature with heading. The data shown is from 4/11/2013 at 100m during the third flight. All time is in Central Daylight Time (CDT).

As atmospheric pressure decreases with height, pressure data were expected to show an inverse relationship to the GPS height fluctuations. By comparing the first and third graph in Figure 8, an inverse relationship can easily be seen between height and pressure. However, this is not always the case with the pressure data collected during this project. Some flights exhibited sporadic pressure jumps, which are believed to be sensor error (Figure 9). Because of these erroneous data, potential temperature was not used, as discussed in the methods section of this paper.

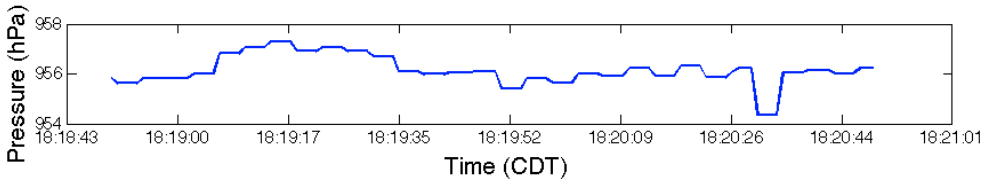


**Figure 9:** A time series of pressure from 4/11/2013 at 100m during the second flight. And anomalous pressure drop can be seen around 18:20:30 CDT.

*Structure Function Parameter*

As discussed in the methods section, there are multiple approaches when it comes to computing the structure function parameter for temperature. These differing techniques result in dissimilar structure function parameter estimates (Figure 10). "Method 1" and "Method 2" represent the first and second technique, respectively. Taylor's hypothesis of frozen turbulence was also considered for each method. "A" implies the method did not utilize Taylor's hypothesis and "B" indicates that it was used. $C_T^2$ values for all separation distances are averaged to result in a singular value for each height. Therefore, if the turbulence is isotropic, homogenous, volume filling, and within the inertial sub range, $C_T^2$ values should be constant over all separation distances. A large variance in $C_T^2$ throughout all separation distances would result in an average that does not fully represent the span of values. Consequently, a flat line is ideal in Figure 10. Four cases, all at 100m have been plotted with all four methods of $C_T^2$ calculation.

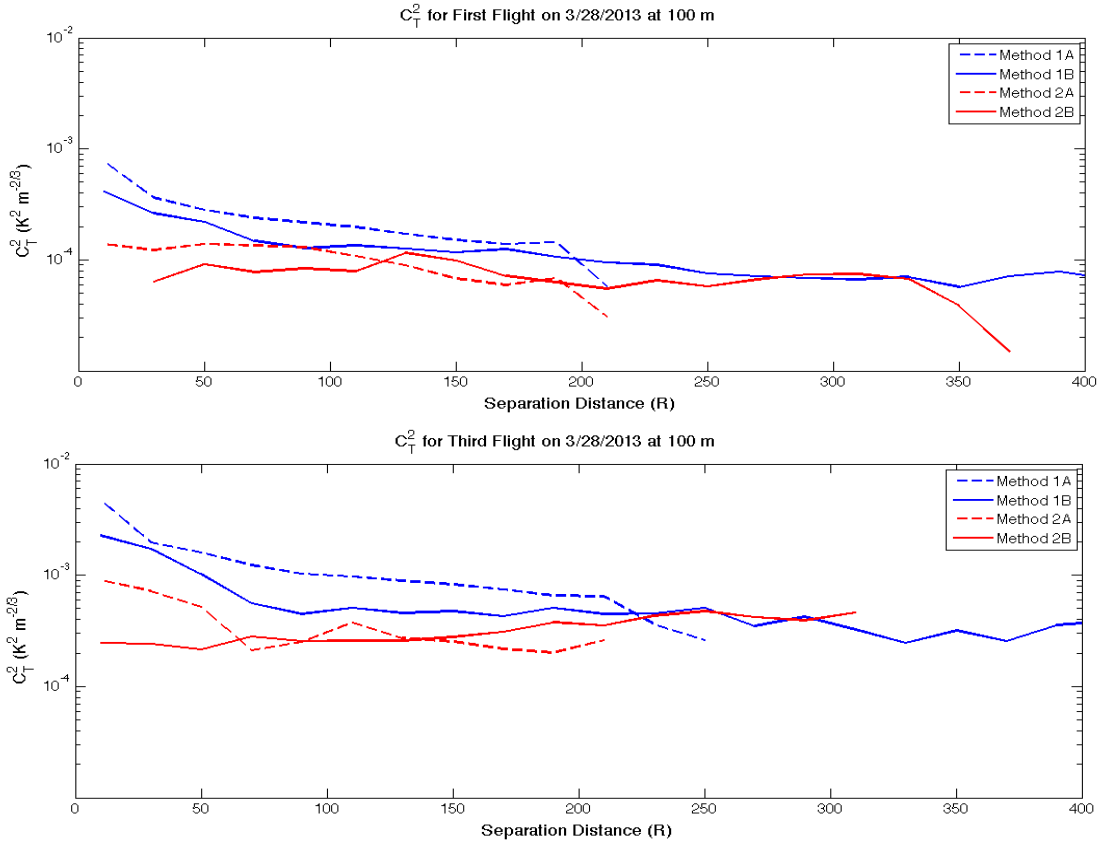


**Figure 10:** Structure Function Parameter ($C_T^2$) plots with respect to separation distance (R) from various flights on 28 March and 11 April 2013 at 100m. Blue and red lines represent Method 1 and Method 2, respectively, as mentioned in the methods section. Solid lines represent the use of Taylor's hypothesis of frozen turbulence. Dashed lines do not utilize Taylor's hypothesis.

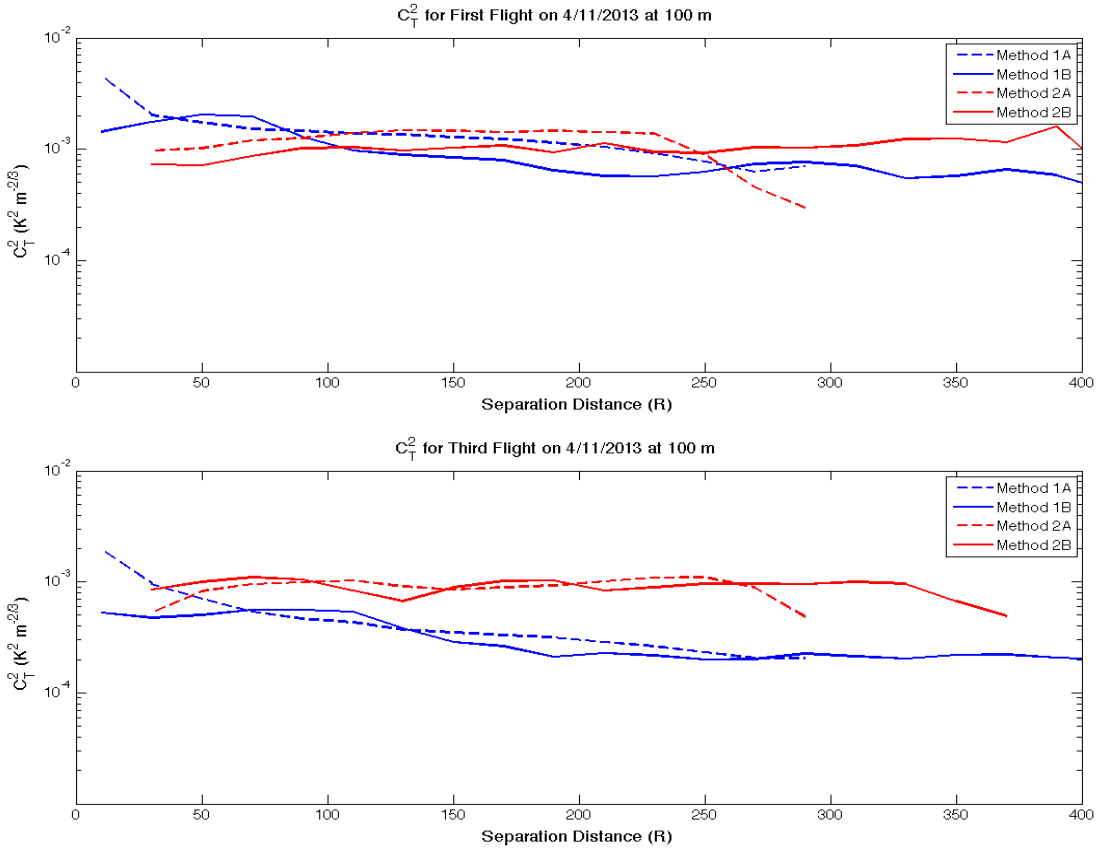


**Figure 10 (cont.):** Structure Function Parameter ($C_T^2$) plots with respect to separation distance (R) from various flights on 28 March and 11 April 2013 at 100m. Blue and red lines represent Method 1 and Method 2, respectively, as mentioned in the methods section. Solid lines represent the use of Taylor's hypothesis of frozen turbulence. Dashed lines do not utilize Taylor's

Average standard deviation (STD), of the four cases mentioned above, is plotted for each method of $C_T^2$ calculation that was discussed in the methods section (Figure 11). Method 2 has a much lower STD than Method 1. This supports our hypothesis that the "moving window method" is better suited for calculating $C_T^2$ as it reduces the error of assuming data are collected simultaneously. Likewise, Taylor's hypothesis of frozen turbulence vastly improved Method 1 and slightly improved Method 2 as well, which proves our theory that Taylor's hypothesis is needed to

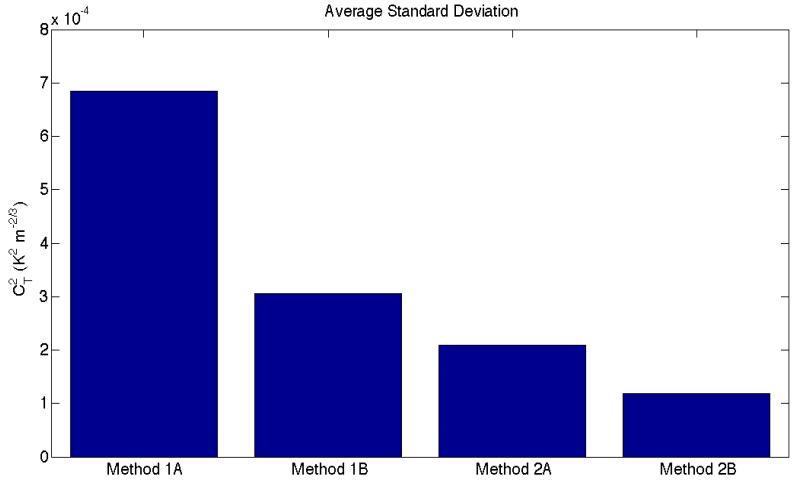


**Figure 11:** Average standard deviation of $C_T^2$ for the four cases in Figure 10 using various methods of calculation.

account for the advection of turbulence when calculating $C_T^2$. Overall, Method 2B has the least deviation of $C_T^2$. Thus, Method 2B will be used for analysis further on in this paper.

*Sodar Comparison*

As mentioned above, $C_T^2/T^2$ can be related to the reflectivity of backscattered acoustic waves if various conditions discussed above are satisfied. Therefore, using an arbitrary calibration constant for the Funjet, simulated reflectivity was calculated using Equation 7. Sodar reflectivity, averaged for the entire flight time, is plotted alongside the simulated reflectivity, for all three days of data collection, for visual comparison (Figure 12).

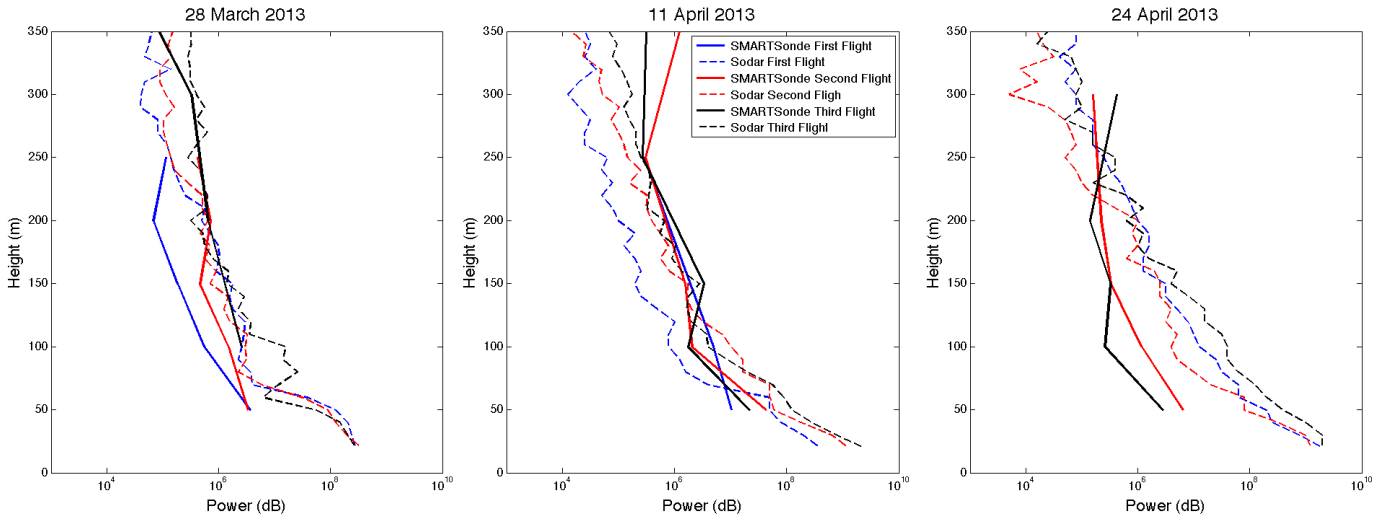


**Figure 12:** Sodar return power shown along with SMARTSonde simulated return power for 28 March, 11 April, and 24 April 2013. Note: The first flight on 24 April began circling at 400 m and increased every 100 m in height, hence the lack of data on the plot.

The proportionality between the actual and simulated reflectivity can be seen. The data collected on 28 March and 11 April appear to have the closest proportionality to the sodar data. However, on 24 April, the data collected for this project does not seem to correlate well with the sodar data. A review of vertical velocity during the flight, using the on-site lidar, reveals strong and persistent updrafts were present during a majority of the flight period (Figure 13). There were updrafts present during the flights on 11 April as well, however, they look more sporadic and less persistent. These updrafts may have a large influence on $C_T^2$ and were not accounted for in this paper.

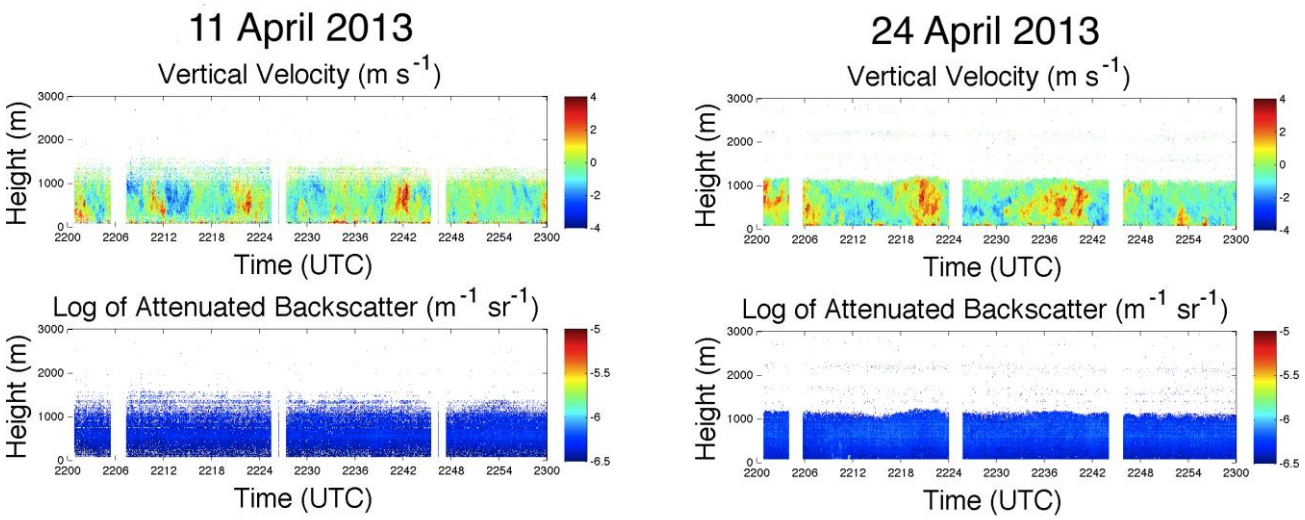


**Figure 13:** Vertical velocity derived from the lidar located at KAEFS for 11 April and 24 April 2013.

## Conclusion

Using the Funjet, an analysis of the feasibility to obtain quantification of atmospheric turbulence was completed. The use of UA to collect in-situ measurements is desirable for meteorological purposes as other means of in-situ data collection are not as flexible and usually only have one style of data collection, i.e. vertical or stationary. The operation of a UA within the National Airspace can be quite complex and requires strict compliance with FAA regulations. However, operating under the first civilian CoA in the state of Oklahoma, this project has proven that the use of autonomous unmanned aircraft, for meteorological data collection, can be safely executed when coordination and communication are a priority.

As was shown in this paper, an atmospheric profile of the PBL can be obtained with the use of a UAS. While similar to what could be obtained from a rawinsonde rising through the atmosphere, the rawinsonde instrument package is rapidly carried up by a balloon, thus, limiting the temporal resolution, unlike a UAS. Not only can the Funjet probe the vertical structure of the PBL, a horizontal flight trajectory allows for spatial temperature variations to be collected. Horizontal gradients in temperature were used to calculate $C_T^2$ to quantify turbulence within the PBL. Four methods of $C_T^2$ calculation were considered and a superior method prevailed. The "moving window method" using Taylor's hypothesis of frozen turbulence showed the most promising results. While results show a UA can be used to obtain the structure function parameter for temperature, more robust methods should be researched.

After calculations of the temperature structure function parameter, a comparison of power from the Funjet and the on-site sodar at KAEFS was done. Out of the three days used in this project, 28 March and 11 April showed a reasonable proportionality between the Funjet simulated reflectivity and the sodar reflectivity. It is believed that thermals may have impacted the $C_T^2$ calculations from 24 April. Further study needs to be conducted on how to account for vertical motion. The problems discussed here will continue to be reviewed, however, it is the consensus of the authors that the use of a UAS for meteorological study is advantageous and has great value in atmospheric science.

## References


Bonin, T., 2011: Development and initial application for the SMARTSonde for meteorological research. M.S. thesis. School of Meteorology, The University of Oklahoma, 113 pp.

Chilson, P.B., A. Gleason, B. Zielke, F. Nai, M. Yeary, P. M. Klein, and W. Shalamunec, 2009: SMARTSonde: A small UAS platform to support radar research. *AMS 34$^{th}$ conf. Radar Meteor*., Boston, Mass. Am. Meteorol. Soc.

Coulter, R.L., and M.L. Wesely, 1980: Estimates of surface heat flux from sodar and laser scintillation measurements in the unstable boundary layer. *Jour. Appl. Meteor.*, **19**, 1209-1222.

Crook N.A., 1996: Sensitivity of moist convection forced by boundary layer processes to low-level thermodynamic fields. *Monthly weather review*, **124**, 1767-1785.

Gossard, E., R. Chadwick, W. Neff, and K. Moran, 1982: The use of ground-based Doppler radars to measure, gradients, fluxes, and structure parameters in elevated layers. *J. Appl. Meteor*., **21**, 211-226.

Holland, G. J., T. McGeer, and H. Youngren, 1992: Autonomous aerosondes for economical atmospheric soundings anywhere on the globe. *Bull. Amer. Meteor. Soc*., **73**, 1987-1998.

Houston, A.L., B. Argrow, J. Elston, J. Lahowetz, E.W. Frew, and P.C. Kennedy, 2012: The collaborative Colorado-Nebraska unmanned aircraft system experiment. *Bull. Amer. Meteor. Soc.* **93**, 39-54.

Kolmogorov A., 1941: Local structure of turbulence in an incompressible fluid for very large Reynolds numbers. *Dokl Akad Nauk SSRR*, **30**, 299-303.

Konrad, T., M. Hill, R. Rowland, and J. Meyer, 1970: A small, radio-controlled aircraft as a platform for meteorological sensors. *Appl. Phys. Lab. Tech. Digest*, **10**, 11-19.

Lenschow D.H. , 1986: Introduction. In *Probing the Atmospheric*

*Boundary Layer*, D. H. Lenschow, Ed. Amer. Meteorol. Soc., Boston, Mass. 201-239.

Lin, P. H., 2006: The first successful typhoon eyewall-penetration reconnaissance flight mission conducted by the unmanned aerial vehicle, Aerosonde. *Bull. Amer. Meteor. Soc.,* **87**, 1481-1483.

Neff, W. D. and R. L. Coulter, 1986: Acoustic remote sensing. In *Probing the Atmospheric Boundary Layer*, D. H. Lenschow, Ed. Amer. Meteorol. Soc., Boston, Mass. 201-239.

Reuder, J., P. Brisset, M. Jonassen, M. Muller, and S. Mayer, 2009: The Small Unmanned Meteorological Observer SUMO: A new tool for atmospheric boundary layer research. *Meteorol.* Z., **18**, 141-147.

Schafer, R., P.T. May, T.D. Keenan, K. McGuffie, W.L. Ecklund, P.E. Johnston, and K.S. Gage, 2001: Boundary layer development over a tropical island during the Maritime Continent Thunderstorm Experiment. *J. Atmos. Sci.*, **58**, 2163-2179.

Shuqing, M., C. Hongbin, W. Gai, P. Yi, and L. Qiang, 2004: A miniature robotic plane meteorological sounding system. *Advances in Atmospheric Sciences*, **21**, 890-896.

Spiess, T., J. Bange, M. Buschmann, and P. Vorsmann, 2007: First application of the meteorological Mini-UAV '$M^2$ AV'. *Meteorol.* Z., **16**, 159-169.

Stephens, G.L., and Coauthors, 2000: The Department of Energy's Atmospheric Radiation Measurement (ARM) Unmanned Aerospace Vehicle (UAV) program. *Bull. Amer. Meteor. Soc.,* **81**, 2915-2937.

Taylor G.I., 1938: The spectrum of turbulence. *Proc. Roy. Soc. London*, **A132**, 476-490.

van den Kroonenberg A.C., S. Martin, F. Beyrich, and J. Bange, 2011: Spatially-averaged temperature structure parameter over a heterogeneous surface measured by an unmanned aerial vehicle. *Boundary-Layer Meteorology*, **142**, 55-77, doi:10.1007/s10546-011-9662-9.

World Health Organization, 2009: Global health risks: Mortality and burden of disease attributable to selected major risks.

Wyngaard, J. C., 2010: *Turbulence in the Atmosphere*, Cambridge University Press, New York,

393 pp.

Wyngaard, J.C., and M.A. LeMone, 1982: Behavior of the refractive index structure parameter in the entraining convective boundary layer. *Jour. Atmos. Sci,* **37**, 1573-1585

Wyngaard , 1986: Measurement Physics. In *Probing the Atmospheric*

*Boundary Layer*, D. H. Lenschow, Ed. Amer. Meteorol. Soc., Boston, Mass. 201-239.